Hydrogen diffusion into three metallurgical microstructures of a C–Mn X65 and low alloy F22 sour service steel pipelines

E. Fallahmohammadi [a], *F. Bolzoni* [a,*], *G. Fumagalli* [a], *G. Re* [a], *G. Benassi* [b], *L. Lazzari* [a]

[a] *Politecnico di Milano, Dipartimento di Chimica, Materiali ed Ingegneria Chimica "Giulio Natta", Via Mancinelli, 7, Milano 20131, Italy*
[b] *Cescor srl, Via Maniago, 12, 20134 Milano, Italy*

Received 28 March 2014
Received in revised form
20 June 2014
Accepted 23 June 2014
Available online 22 July 2014

Introduction

Sour service pipeline steels are produced in a very large quantity for the construction of pipelines to export hydrocarbons from oil&gas fields. At the same time increasing energy demand has driven the development of new oil and gas fields around the world, many of which are sour; moreover, many old wells are increasingly turning sour. Therefore, about 40% of the world's natural gas and oil reserves are categorized as sour. In this scenario, sour environment corrosion becomes one of the most challenging problems in the use of steel pipelines.

The cathodic reaction in sour corrosion produces hydrogen, which succeeds in penetrating into ferritic steels impairing their toughness and promoting different kinds of brittle behaviour (e.g., hydrogen induced cracking HIC, sulphide stress cracking SSC, stress oriented hydrogen induced cracking SOHIC).

* *Corresponding author*. Tel.: +39 02 2399 3151; fax: +39 02 2399 3180, +39 02 2399 3080.
E-mail address: Fabio.bolzoni@polimi.it (F. Bolzoni).

The presence of hydrogen in the metallic materials can be also due to cathodic protection, treatments like pickling, galvanic coating, welding in humid environment. Moreover, hydrogen can be absorbed into metals in pressure vessels containing high pressure hydrogen gas.

Due to its very small diameter, atomic hydrogen can diffuse even through high thickness steel walls causing embrittlement into the material core, hence hydrogen diffusion kinetics becomes a very important aspect of hydrogen embrittlement of steels.

Hydrogen transport through a steel wall is the combination of two different phenomena, i.e.: purely physical diffusion driven by concentration gradient, described by Fick's laws and physicochemical reactions with specific microstructural sites, called traps, which have binding energies with hydrogen higher than regular interstitial sites. Traps are usually classified as reversible or irreversible depending on the binding energy with hydrogen and practically speaking we can also say that reversible traps, associated with low binding energies, can release hydrogen at room temperature when the surface concentration goes to zero, i.e., when corrosion is no more active; on the contrary irreversible traps, associated with high binding energies, can only release hydrogen at temperatures higher than ambient one. Traps can also be classified as saturable if they can retain only one hydrogen atom (or a defined finite number) or not saturable if they can accommodate any quantity of hydrogen (e.g. blisters). Vacancies, dislocations, grain boundaries, interfaces of the matrix with precipitates or inclusions, certain alloying elements such as titanium, and so on, have been identified as trapping sites, each of them having a specific binding energy and reaction parameters.

Many authors have studied the effect of steel microstructure on hydrogen diffusion, however, because so many parameters are involved in the phenomenon, a comparison of that available results is very difficult. Different concentration values and diffusion-related parameters can be used to characterize hydrogen interactions with steel: in the following results obtained in our experimental activity are discussed on the basis of a literature review on the diffusion coefficient .

In fact, the diffusion coefficient is a unique parameter which completely describes the permeation of hydrogen in the pure diffusion model that follows Fick's laws. Moreover, it is a material characteristic and it is constant during permeation tests carried out using the Devanathan and Stachurski method [1]. On the contrary when hydrogen trapping occurs, only an apparent diffusion coefficient can be evaluated. The reaction of hydrogen with trapping sites is the basis of many mathematical models, e.g. McNabb and Foster [2], Oriani [3], Iino [4,5], Peter et al. [6], Leblond and Dubois [7,8]. In summary, the apparent diffusion coefficient depends on number and binding energy of trapping sites, the kinetics of capture and release of hydrogen in any kind of traps. Furthermore, from the available models it can be concluded that when hydrogen trapping takes place the apparent diffusion coefficient is not constant and varies during the permeation transient (permeation curve shifts toward longer times and is less steep than the one obtained in the case of pure diffusion).

Lastly, it is possible to separate the contribution of reversible and irreversible traps using the method of repetitive permeation tests proposed by Turnbull [9] and ISO [10]. During the first permeation test both reversible and irreversible traps react with hydrogen atoms flowing from the cathode to reach equilibrium conditions. During the subsequent discharge only reversible traps can release the trapped hydrogen and can react again during any following tests, while irreversible traps don't interfere any more in the diffusion process.

A review of the diffusion data obtained by different authors on API pipeline steels is reported in Table 1. Some diffusion parameters for API steel grades ranging from X52 to X100 are reported: for the same steel grade, when the number of data is large enough (e.g. X65 or X70), the diffusion coefficient D may vary by a factor larger than 10 and, with the exception of X52, there is a tendency by which D decreases as steel grade increases. Reference [11] reports diffusion-related measurements, using the electrochemical method suggested by Devanathan and Stachurski [1], on two X70 grade steels, one as standard and the other as a low Mn content, respectively; specimens were taken at different stages of production and from different sections of the hot rolled plate (centreline and edge); the correlation of testing results to steel microstructure suggested the following considerations:

- Equations taken from the literature, often used to calculate D, lead to different values, as Turnbull already reported [12];
- values of D obtained from breakthrough times are larger than those calculated from lag times, i.e., the apparent diffusion coefficient at the beginning of current transient is larger than the one at the end;
- values of D calculated from breakthrough times during the second permeation are slightly larger than the ones of the first permeation; this result fits with the theory of Turnbull [9,12] also reported in the ISO standard 17081 [10]; instead, when calculated from lag times this trend is not confirmed, being D values of second permeation slightly lower than the first;
- for the studied materials, diffusivity decreases if the grain size decreases and/or the dislocation density and the content of (Ti,Nb)C,N precipitates increase.

Park et al. [13] found that in a linepipe steel analogous to API 5L X65 grade, the diffusion coefficient when microstructure is ferrite (F)/degenerated pearlite (DP) is larger than when microstructure isferrite/acicular ferrite (AF) or ferrite/bainite (B); authors concluded that the hydrogen trapping efficiency increases in the order DP < B < AF. It must be observed that microstructures displaying the highest values of D are also the ones with the lowest fraction of hard constituents, which seem to be responsible for the decrease of diffusion coefficient although it is difficult to say if the extent of this effect depends more on the type or on the quantity of these hard constituents. Lastly, the value of D of the F/AF or F/B microstructure ($\approx 4 \cdot 10^{-10}$ m^2 s^{-1}) is only slightly larger than the one obtained on a similar steel by Haq [11] while the one obtained on the F/DP microstructure is much larger ($\approx 9 \cdot 10^{-10}$ m^2 s^{-1}).

On the other hand, Dong et al. [14,15] found for D a value of $2.63 \cdot 10^{-11}$ m^2 s^{-1} in an API 5L X65 steel having polygonal ferrite with a small amount of acicular ferrite (F/AF) and same authors reported in Ref. [15] a measured D value of $1.04 \cdot 10^{-12}$

Table 1 – Summary of permeation parameters for pipeline steel in literature; cathodic i_c = current density (mA cm^{-2}), th. = thickness (mm); D_{app} = (10^{-10} m^2 s^{-1}); C = (mol H m^{-3}).

Ref	Steel	Charging solution	i_c	th./coating	Microstructure	Method	D_{app}	C
[14]	X70	0.5 M H_2SO_4 +	0.5	0.77/Ni	F + AF	t_{lag}	0.263	28.8
[15]	X100	250 mg/L $NaAsO_2$	10		F + B	t_{lag}	0.01	134
[13]	X65	NACE	0.5	1/Pd	DP/AF/B, MA	t_b	4–9.4	13–28
[36]	X70	NACE	pH_2S	1/Pd	F + DP + AF, F + AF + BF	t_b	0.5–4.3	–
[20]	X52	NACE	OCP	0.5/Pd	F + P, AF + P	t_b	0.15–0.24	–
[37]	X65	0.1 N NaOH	2–4	0.6 to 2.5/–	Q&T	t_{lag}	0.9–0.96	5.7
[38]	X65	NACE	OCP	1/-	F + P	t_b	2.4	20.1
					B + M/A	t_b	1.1	5.5
					F + P	t_{lag}	2.5	15.6
					B + M/A	t_{lag}	1.2	–
[39]	X80	0.5 M H_2SO_4	10-50	0.5/Pd	F + BF + M/A	t_{lag}	0.2	26
[40]	X70	0.1 NaOH	–	–/Pd	F + P + M	t_{lag}	0.73–0.79	–
[11]	X70 Edge	0.1 N NaOH + $Na_2S{\cdot}H_2O$	3.5	–	F + P	t_{lag}	1st 1.97 ± 0.09 2nd 1.77 ± 0.06	0.84
	X70 Centreline				F + P	t_{lag}	1st 2.25 ± 0.19 2nd 2.06 ± 0.17	0.74
	MX70 Edge				F + P	t_{lag}	1st 1.70 ± 0.04 2nd 1.57 ± 0.03	1.2
	MX70 Centreline				F + P	t_{lag}	1st 1.71 ± 0.01 2nd 1.52 ± 0.03	0.90
	X70 TB Edge				F + B	t_{lag}	1st 2.10 ± 0.19 2nd 1.33 ± 0.31	0.80
	X70 TB Centreline				F + Granular B	t_{lag}	1st 3.05 ± 0.17 2nd 2.15 ± 0.30	0.77
	Normalized TB				F + P	t_{lag}	1st 4.01 ± 0.02 2nd 3.82 ± 0.13	0.60
[23]	ASTM SA182 F22	0.5 M H_2SO_4 + 200 ppm As_2O_3	0.05	1.5/Pd	M	t_b	4.47 ± 0.24	–
					B	t_b	5.19 ± 0.39	–
					F + globular B	t_b	40.00 ± 2.98	–
[41]	SAE 1008	0.1 N NaOH	Pot. Static –1100 mV SHE	1/–	F + fine P	t_b	1st 2.19 ± 0.11 2nd 2.62 ± 0.15	–
					F + fine globular C	t_b	1st 3.47 ± 0.11 2nd 3.94 ± 0.25 3th 4.18 ± 0.18	–
					F + fine carbides	t_b	1st 6.43 ± 0.40 2nd 7.78 ± 0.39 3th 8.01 ± 0.32	–
[34]	Mild Steel	0.1 N NaOH + 1 g L^{-1} $Na_2S{+}9H_2O$	10	1/Ni	Annealed	t_{lag}	10.5	0.44
	S45C				Annealed		2.96	1.18
	S45C				Normalized (P + F)		2.78	1.29
	S45C				Spheroidized		3.50	1.13
	S45C				Quenched (M)		0.37	4.92

F: Ferrite, AF: Acicular Ferrite, B: Bainite, DP: Degenerated Pearlite, MA: Martensite/Austenite, P: Pearlite, BF: Bainitic Ferrite, GB: Granular Bainite, Q&T: Quenched and Tempered, OCP: open circuit potential, 1st and 2nd : stand for 1st and 2nd polarization tests.

m^2 s^{-1} in API 5L X100 steel with a bainitic/ferritic microstructure; these authors confirmed that diffusion coefficient decreases as steel grade increases, even if the specific values measured were at least 10 times lower than the one obtained by other authors on similar materials.

Kappes et al. [16] measured on an X65 pipeline steel in solutions containing thiosulfate or hydrogen sulphide in variable concentrations, D values of the order of 10^{-10} m^2 s^{-1} but dependent on the environment. Authors attributed this effect to trapping and ascribed divergences in the apparent diffusion coefficients in terms of trap occupancy fraction, which increases with hydrogen concentration in the lattice.

Bolzoni et al. [17] considered also the effect of different orientation of specimens with respect to the rolling direction for a ferritic/perlitic X60 grade steel and a ferritic/bainitic X100 grade steel, finding that diffusion coefficient of X100 is always lower than that of X60 and that transverse rolling direction is more favourable to diffusion compared to the longitudinal one for X60, while the more homogeneous X100 steel doesn't show a significant effect of orientation.

Cabrini et al. measured diffusivity for different pipeline steels [18,19]. Apparent diffusion coefficient in their tests increased for control rolled steel with respect to hot rolled steel; authors attributed this effect to the finer ferritic grain. In the same research, hot rolled steels of recent production showed much lower diffusivities than similar steel grade (X60) produced in '60s, with rather high content of carbon and sulphur and coarse microstructure with very pronounced pearlite band [18,19].

Table 2 – Heat treated steel samples: micro-hardness and percentage of inclusion area are given.

Designation	Materials	Heat treatment	Microhardness (HV)	% Of inclusion area
WQ	X65	930 °C-30 min-WQ	433 ± 33	0.095 ± 0.05
	F22	930 °C-30 min-WQ	478 ± 15	0.034 ± 0.009
FC	X65	930 °C-30 min-FC	150 ± 18	0.125 ± 0.02
	F22	930 °C-30 min-FC	170 ± 11	0.042 ± 0.011
Q&T	X65	As received	206 ± 7.9	0.102 ± 0.037
	F22	As received	211 ± 3.8	0.045 ± 0.015

Serna et al. reported in Ref. [20] that permeation curves of an X52 grade steel follow the theoretical Fick's model at 50 °C while at 25 °C the curves are much less steep, more irregular and similar to the ones predicted for example by the Iino's model with reversible and irreversible traps [4,5], concluding that the probability of hydrogen trapping is lower at higher temperature, where hydrogen permeation is controlled by lattice diffusion.

Asher and Singh [21] measured the diffusion coefficient on an X65 grade steel with an unusually high carbon content (=0.25%, near the upper limit of API 5L specification [22]) in three different microstructures: *D* increased in the following order: quenched martensitic structure, as received ferrite/pearlite, normalized coarser ferrite/perlite. Moreover, the diffusion coefficient of quenched samples increased as tempering temperature increased. These results confirm that in this type of steels the apparent diffusion coefficient increases with coarser and more relaxed microstructures.

The same behaviour was found by Parvathavarthini et al. [23] on 2.25% Cr–1% Mo ferritic steel. These Authors treated the steel in different ways by quenching, air-cooling, furnace-cooling, air-cooling and tempering at different temperatures and for different times. The diffusion coefficients measured were inversely correlated to the Vickers macro-hardness of the material.

The effect of grain size on hydrogen diffusion in X70 grade steel was studied by Yazdipour et al. [24] who found that *D* increased as grain size increased, up to a maximum at 46 μm, then followed by a decrease of *D* for larger grains. This behaviour was explained assuming that grain boundaries have a twofold effect on either diffusion rate or as trapping sites: the two effects result in a maximum in the diagram of the diffusion coefficient vs. grain size.

In the present work, we studied the diffusion process in a pipeline steel in three different metallurgical microstructures by means of different experimental methods in order to better investigate the effect of pure (lattice) diffusion and trapping. The different measurement methods adopted to evaluate hydrogen diffusion coefficients are: 1) charge method; 2) partial charge and partial discharge method; 3) discharge method [25].

Experimental procedure

Chemical composition and mechanical properties of the steel in as received conditions

Permeation tests were carried out on C–Mn micro-alloyed X65 steel and low alloy 2.25 Cr 1 Mo steel samples which have been extracted from a seamless linepipe [26–29].

The X65 grade steel in as received conditions was produced by quenching and tempering in order to fulfil the specification API 5L X65 grade and consists of a C–Mn steel micro-alloyed with Nb and V with a small amount of Cr, Mo and Ni to improve hardenability and Ca for inclusion shape control.

The F22 steel was a low alloy steel and produced by quenched and tempering. Its good mechanical properties rely on a fine dispersion of molybdenum carbides and amount of chromium that increases corrosion properties.

The materials are for sour service use, therefore it underwent through all the required qualifications. In Table 3 the chemical composition of these material is reported. In Table 4 tensile test results of X65 and F22 at room temperature in as received condition are reported.

Metallurgical microstructures

The microstructure of both steels was examined using optical and Scanning Electron Microscope (SEM).

As received X65 steels consists in ferrite with finely dispersed carbides (mainly at grain boundaries) and tempered lath martensite (Fig. 1(a,b)), it is rather homogeneous, no significant variations are visible among different alignments (internal, centre, external) or for different orientations (longitudinal, transversal). Inclusion shape is round (type D globular inclusions), as it is expected for a sour service material treated with calcium. The microhardness value is 206 ± 7.9 HV, while the grain size is 7 ± 0.2 μm.

Microstructure of F22 steel is homogeneous and is constituted by mixed tempered martensite and ferrite with dispersed carbides (Fig. 1(c,d)). Inclusion density is very low; material has been treated with calcium and inclusion shape

Table 3 – Chemical composition (weight %) of X65 and F22 steels.

Steel	C	Mn	S	Mo	Cr	Ni	Nb	V	Ti
X65	0.11	1.18	0.007	0.15	0.17	0.42	0.023	<0.06	<0.01
F22	0.14	0.43	0.001	1.04	2.25	0.08	0.02	<0.01	<0.01

Table 4 – Some mechanical properties of as received X65 and F22 steels.				
Materials	Yield strength	Ultimate tensile strength	Young's modulus	Elongation
X65	511 ± 6.7 MPa	609 ± 5.7 MPa	206 ± 6.0 GPa	21 ± 6.5%
F22	468 ± 2.7 MPa	592 ± 2.1 MPa	206 ± 1.5 GPa	20 ± 2.5%

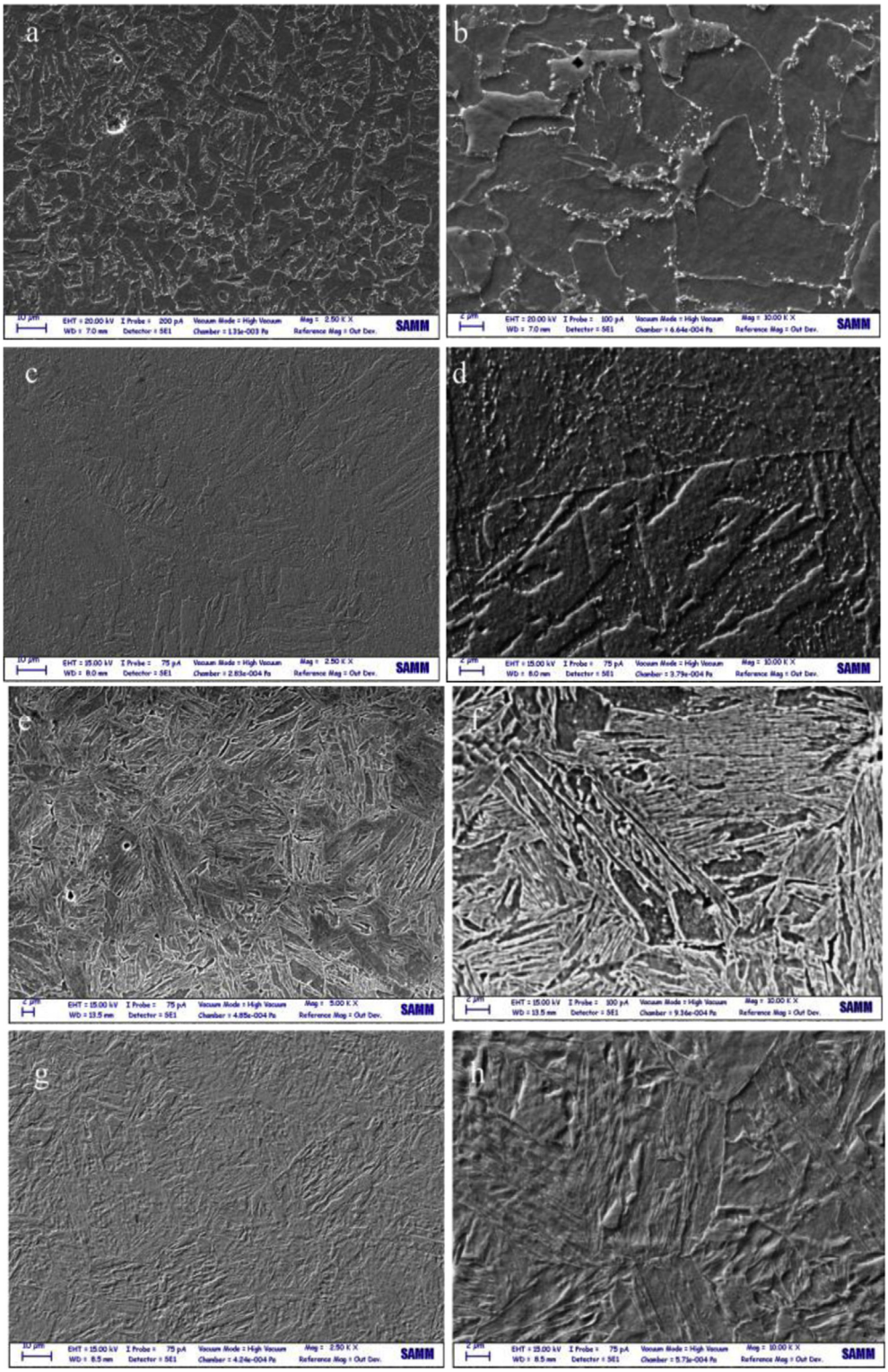

Fig. 1 – SEM micrographs of the steel microstructures. As received, i.e. Q&T: X65 (a,b), F22 (c,d); Quenched: X65 (e,f), F22(g,h); Annealed: X65 (i,j), F22(k,l).

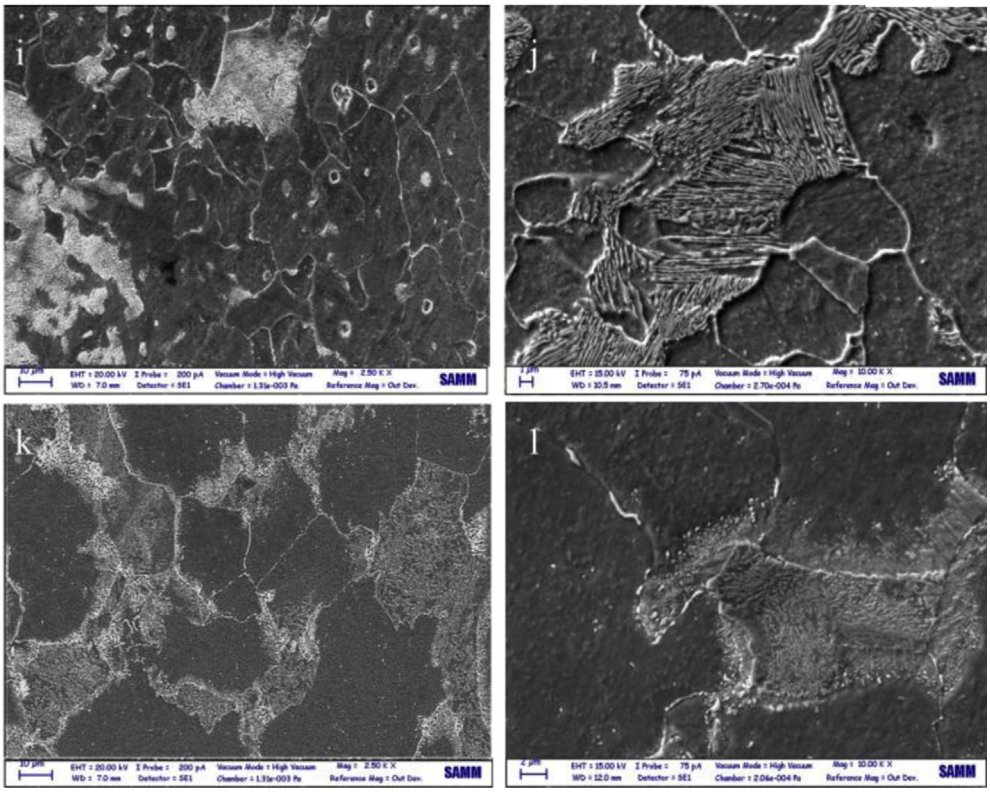

Fig. 1 – (*continued*).

is round (type D globular inclusions) and no elongated inclusions are present; longitudinal and transverse orientation don't show any difference neither as inclusion density nor as mean diameter (1.2 μm longitudinal surface, 1.3 μm transversal surface); no central segregation is present. The F22 had homogenous hardness measurements along the thickness of 211 ± 3.8 HV and the grain size was 4 ± 0.5 μm.

In order to evaluate the effect of microstructure on material diffusion properties, some samples (about 1.5 mm thick) were fully quenched, while other samples were annealed. Quenching was performed by treatment at 930 °C for 30 min and rapid water cooling.

As shown in Fig. 1(e,f), the microstructure of X65 quenched steel, is almost completely martensitic and for F22 constitutes of martensite (Fig. 1(g,h)) with a microhardness equal to 433 ± 33.7 HV for X65 and 478 ± 15 for F22.

Annealed samples were austenitized at 930 °C for 30 min and afterwards the furnace was switched off, to allow slow cooling of samples to room temperature. The microstructure after annealing, shown in Fig. 1(i,j) for X65, consists of ferrite grains of not homogeneous dimensions and islands of pearlite. In the case of the annealed F22 steel, Fig. 1(k,l), ferrite and fine pearlite with a chromium carbide precipitate in grain boundaries were observed. The microhardness value is 149.8 ± 19.2 HV and the grain size is 12 ± 1.5 μm. The mean value of percentage of inclusion for annealed samples is 0.1% with a standard deviation of 0.02. As it is shown in Table 2, the density of inclusions is almost the same for all the microstructures analyzed, as expected, because heat treatment should not alter this constituent: therefore, the effect of non-metallic inclusions on hydrogen diffusion should be the same for the different steel microstructures here examined.

Surface preparation of specimens

The permeation test membranes are samples with dimensions ≈20 × 40 mm^2 and 1.3 ± 0.15 mm thick, obtained by cutting a piece of pipe perpendicular to its radius in order to simulate hydrogen radial diffusion. The surfaces were then prepared in the following way:

1. mechanical grinding of both surfaces with emery papers of decreasing SiC particle dimensions down to 1200 grit (water as cooling medium);
2. brazing of copper electrical connection;
3. cleaning of the sample with ethyl alcohol;
4. masking the surface with kapton® tape, with a free square area ≈2.2 cm^2 in the anodic side;
5. pickling in 37% HCl until uniform and copious hydrogen evolution is reached (few seconds);
6. application of palladium coating (≈0.1 μm homogeneous and adherent layer) by electrodeposition in 28.5% NH_4OH + 5 gL^{-1} $PdCl_2$ solution with cathodic current of 2 mA (*E* vs Ag/AgCl = −1.00 V) for 5 min;
7. cleaning with distilled water and ethyl alcohol;
8. removal of masking tape and cleaning with trichlorethylene;
9. mechanical grinding of cathodic surface with 1200 grit emery paper and final cleaning with ethyl alcohol.

Experimental apparatus

Permeation experiments were carried out on a modified Devanathan and Stachurski's cell [1], according to ISO 17081 [10], as it is illustrated in Fig. 2(a). The apparatus is composed by two glass compartments; polycarbonate and polyvinyl chloride junction caps, were used between the two compartments which held the samples, and Viton® O-rings were applied for sealing. The sample area exposed to the cathodic solution (entry side of hydrogen) was 1.54 cm^2, the ratio between anodic and cathodic area was 0.9, which corresponds to a radius-thickness ratio of 5:1 as recommended by the standard [10]. Cathodic and anodic solutions were thermoregulated at constant temperature of 20 ± 2 °C.

The cathodic solution used in all the experiments was 0.4 mol/L of acetic acid (CH_3COOH) and 0.2 mol/L of sodium acetate (CH_3COONa), buffered at pH = 4.2. A peristaltic pump (flow rate = 8.5 L/h) guaranteed a continuous flow of the solution to the cathodic surface with a velocity at the tip of the inflow tube of about 1 m/s (Fig. 2(b)) minimizing the alkalization of the cathodic surface. In order to have a sufficient solution turnover, the pump took the acetic solution from a 5 L reservoir where the solution was purged by dry nitrogen in order to reduce oxygen content. It is worth mentioning that the pump was enclosed in a Faraday's cage, due to the system sensitivity to the electric alterations.

The reference electrode used in this part of the cell was double junction Ag/AgCl/3 mol/L KCl//(E ≈ 0.20 V vs. SHE at 20 °C), the counter electrode was a platinum wire with a surface of about 1.5 cm^2. The tube used to carry the solution to the cell also had the function of Haber-Luggin capillary (Fig. 2(b)).

The anodic cell was filled with 250 cm^2 of stagnant 0.2 mol/L NaOH solution; this solution was not de-aerated. A double junction Hg/HgO/2.5% KOH//(=0.446 mol/L) reference electrode was used, its potential was −0.08 V vs. Ag/AgCl/3 mol/L KCl//. The counter electrode was the same of the cathodic cell.

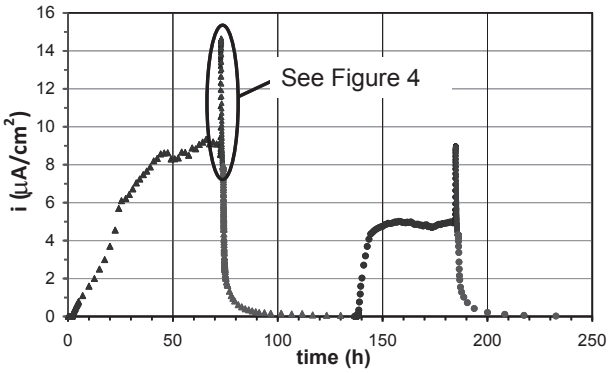

Fig. 3 – Complete permeation test (As received X65).

Permeation procedure

The procedure adopted for the permeation measurements was designed in order to obtain, two permeation transients per complete tests, as suggested by ISO 17081 [10] and two partial transients according to the method proposed by Zakroczymski [31,32]:

1. The sample has been assembled in the cell, the anodic compartment was filled with NaOH solution, anodic polarization of 0.1 V vs. Ag/AgCl was performed and the current has been measured until a current density lower than 0.1 μA/cm^2 was reached. During passivation of the anodic surface, the cathodic compartment was maintained under dry nitrogen flow.
2. While the anodic current density was continuously measured, the other compartment was filled with acetic solution and the cathodic side of the sample was polarized (galvanostatic) at constant current density of −0.5 mA/cm^2. This testing phase lasted until the stabilization of the anodic current and of the cathodic potential was reached, i.e. about 100 h (first charge).

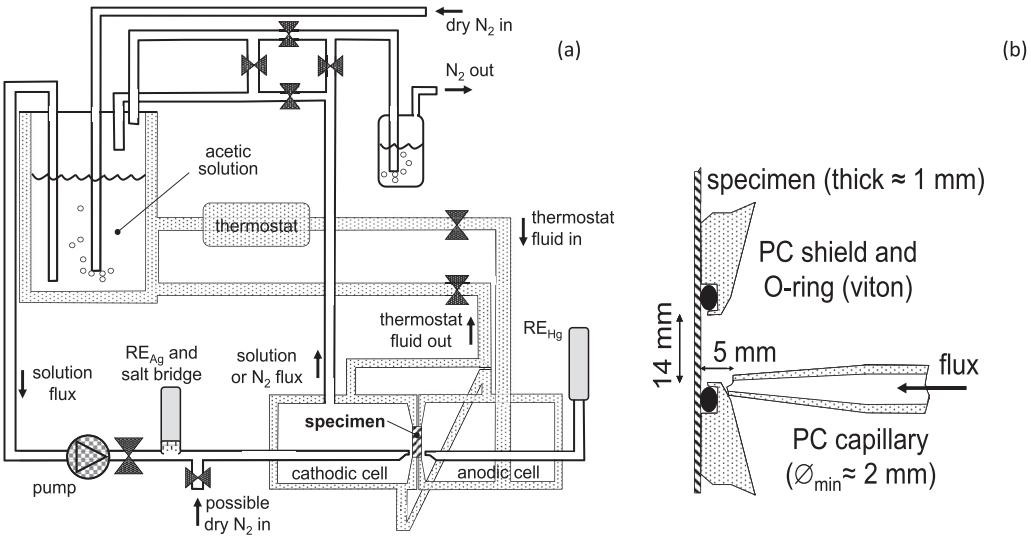

Fig. 2 – Process flow diagram of the experimental apparatus (a); Luggin capillary tube scheme used for the cathodic solution input and for potential measurement (b).

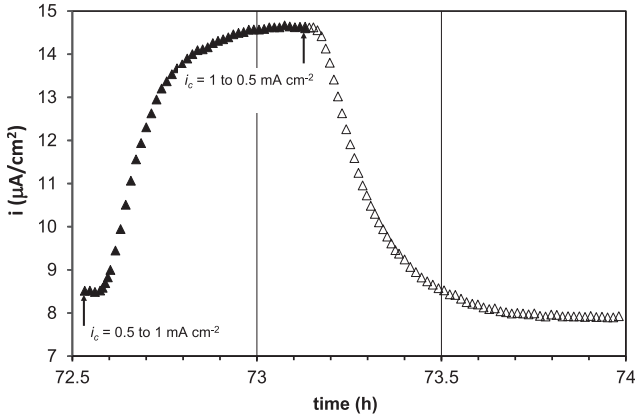

Fig. 4 – Highlight of permeation test of first partial build-up and partial decay. Arrows show when the cathodic current density (i_c) change.

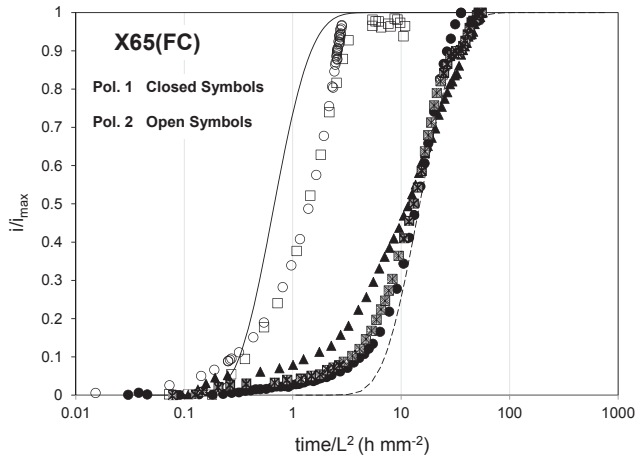

Fig. 5 – Normalized first (closed symbols) and second (open symbols) permeation curves of annealed sample, theoretical curves (continuous lines) are drawn for the two extreme *D* values reported in Table 5 for X65. Thickness range 1.3–1.6 mm.

3. When almost steady state conditions were reached, the cathodic current density was increased from −0.5 mA/cm^2 to −1 mA/cm^2 and then kept constant until the anodic current reached quasi-stationary conditions. This phase lasted less than 2 h (partial charge).
4. Cathodic current density was then decreased from −1 mA/cm^2 to −0.5 mA/cm^2. This phase lasted less than 2 h until a new steady state was reached (partial discharge).
5. Finally, cathodic polarization was interrupted. The anodic current density was continuously measured until passivity was achieved (<0.1 μA/cm^2). This phase lasted some tens of hours (complete discharge).
6. The complete procedure was repeated on the same sample, from point 2 to point 5.

These measurements are very sensitive to physicochemical variations of the cathode, therefore every single part of the experimental procedure was optimized in order to avoid perturbation in the anodic current density. For this reason, for example during complete discharge phase, cathodic compartment emptying and surface drying were carried out not immediately after current switch off, but when the anodic current felt below about 70% of the steady state current (15–20 min). During this time the cathodic current density is not zero but it is equal to the corrosion current that is at least one order of magnitude lower than the previous polarization current.

Results and discussion

Permeation tests

A typical permeation test result is reported in Fig. 3 for a specimen in "as received" metallurgical microstructure. In particular, the anodic current density (μA/cm^2) versus time (h) graph illustrates the first and second permeation versus charge transients, partial transients and complete decays, respectively. Note that a complete test lasted 200–250 h (230 h in the reported example). In Fig. 4 the first partial charge and partial discharge of the same test are highlighted.

The anodic current density was calculated as the difference between measured total anodic current density and passivity current density reached during passivation (i_p < 100 nA/cm^2). In the following, test results will be represented in i/i_{max} vs. time/L^2 graphs, which means that current density is divided by the maximum current density reached during its respective permeation history (dimensionless parameter) and time is divided by the square of the sample thickness (not dimensionless parameter). This elaboration was done in order to eliminate the dependence of experimental data on maximum current peak and sample thickness.

Table 5 – D_{max} and D_{min} values of charge method for different microstructures.

	Microstructures	D_{min} (10^{-11} m^2 s^{-1})	D_{max} (10^{-11} m^2 s^{-1})	D_{max}/D_{min}
X65	Annealed	0.27	5.69	21.07
	Quenched & tempered	0.32	2.20	6.87
	Quenched	0.67	3.82	5.70
F22	Annealed	0.28	8.22	29.8
	Quenched & tempered	0.13	1.37	10.53
	Quenched	0.10	1.00	9.67

Evaluation of diffusion coefficients with charge method

In Fig. 5, permeation curves during first and second charge are reported for annealed X65 sample. Two theoretical curves in continuous lines are also reported, representing the solution of the Fick's second law with typical boundary conditions of this kind of tests, i.e.: zero hydrogen concentration on all membranes at $t = 0$, for $t > 0$ constant cathodic surface concentration, zero anodic surface concentration. Both theoretical curves are calculated with constant diffusion coefficient ($D_{max} = 5.7 \cdot 10^{-11}$ m^2 s^{-1} $D_{min} = 0.2 \cdot 10^{-11}$ m^2 s^{-1}). In this kind of representation, a lower D shifts the corresponding curve to the right (longer time) compared to a curve with higher D. The curves referred to the other specimens with the same microstructures (three specimens) are between the two theoretical curves. Similar considerations apply for the others microstructures.

Theoretical curves don't fit experimental data, which fall in between the two curves, so that a single D_{app} value cannot be used to interpolate a complete experimental permeation curve, as already discussed in the introduction. In Table 5 the extreme values, D_{max} and D_{min}, obtained with the ISO method on various specimens are reported for the three different microstructures here studied (i.e., annealed, quenched and tempered, quenched).

These values are more than one order of magnitude lower than lattice diffusion coefficient for pure iron, as reported in literature ($7.2 \cdot 10^{-9}$ m^2 s^{-1} @ 23 °C [9]).

The histogram in Fig. 6 reports the D_{app} values for annealed samples calculated at different i/i_{max} (i.e., 1%, 3.55%, 10% and 63%). Data confirmed the dispersion of D_{app} value obtained on a single sample, as previously discussed. Moreover, a decreasing trend in the apparent diffusion coefficient with i/i_{max} was always observed, with the highest values for $D_{1\%}$ and the lowest values for $D_{63\%}$. This trend was observed for all microstructures examined in this study, and it can be explained considering that both reversible and irreversible trapping reactions slow down hydrogen permeation, as predicted by theoretical models when trapping effect applies [2–9,12].

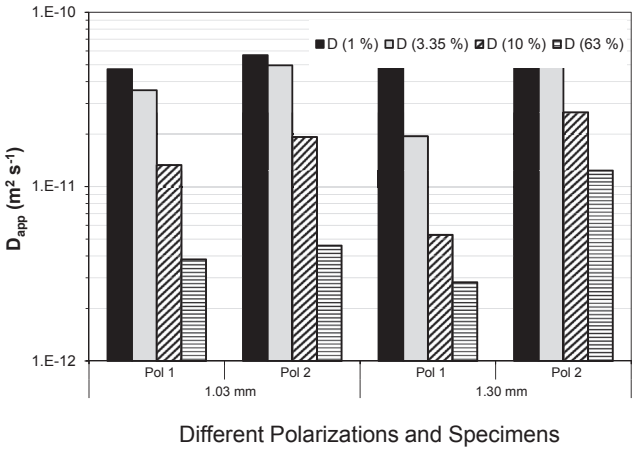

Fig. 6 – Histogram of the D_{app} values for two annealed specimens during first and second charge.

Fig. 5 also shows that the first permeation curve is slower than the second one. This coincides with Turnbull [9,12] results for martensitic steel, although less relevant in the present case.

Experimental tests here reported demonstrate that hydrogen diffusion measurements carried out according to the ISO standard 17081 on a steel of normal commercial production give a rather complex result. Actually, this kind of steel contains many types of inclusions, impurities and inhomogeneities which act as traps and affect hydrogen movement through the material. Therefore, the permeation curve is the results of diffusion process controlled by Fick's laws and physico–chemical reactions of hydrogen with traps of different types like: reversible, irreversible, saturable, not saturable traps, and so on; this impedes to define a complete permeation curve using a single constant parameter. The apparent diffusion coefficient is the results of many processes characterized by different kinetic parameters and it may vary by more than an order of magnitude in a single test run when it is calculated for different values of the ratio i/i_{max}. The adoption of the D value at $i/i_{max} = 0.63$ is a way to compare different test results.

The discharge phase, or desorption of absorbed hydrogen into the membrane (switch-off of the cathodic current) made of the same annealed specimen is also shown in Fig. 7. The experimental curves don't fit the theoretical one obtained by Nanis and Namboodhiri from Fick's laws [30]. Nevertheless,

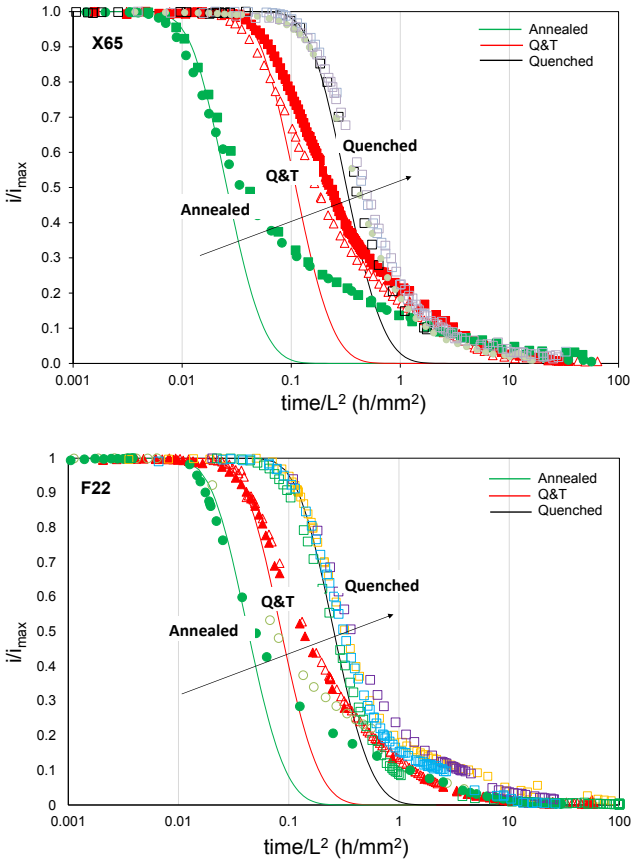

Fig. 7 – Normalized complete hydrogen discharge curves for different steel microstructures of X65 and F22 steels. D values in legends are given in m^2 s^{-1}.

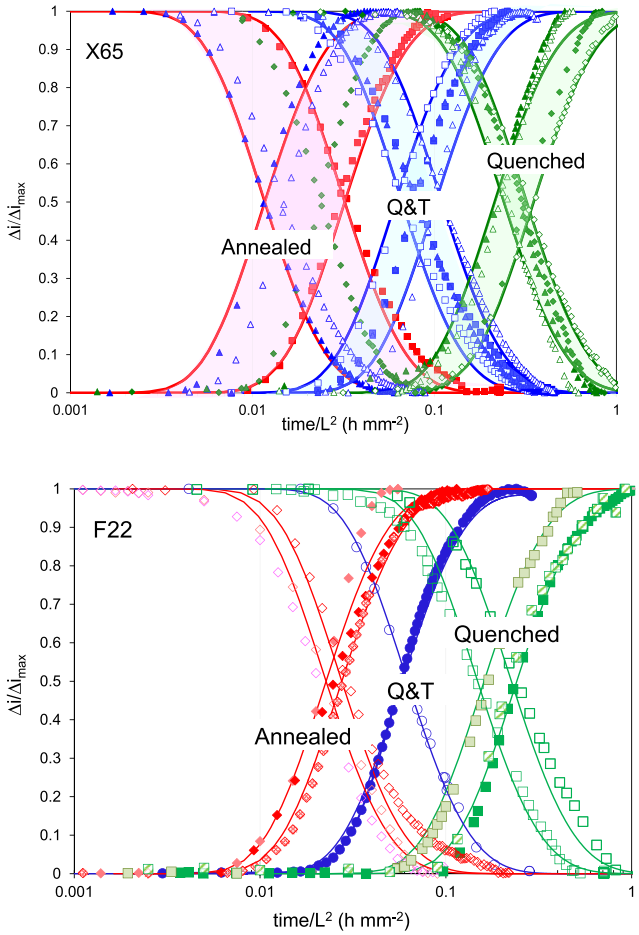

Fig. 8 – Normalized first (solid symbols) and second (empty symbols) partial charge–discharge curves of all samples. Continuous lines are the extreme theoretical curves.

according to Zakroczymski [31,32] and Frappart [33], in the initial part of the curve (roughly in the range $1 \geq i/i_{max} > 0.9$) desorption of diffusible hydrogen prevails and this part of the curve is well described by the theoretical Fick's law with a calculated diffusion coefficient higher than the one derived by permeation curves described above. Hydrogen released from traps becomes perceptible after some seconds, while after few minutes diffusible hydrogen is almost over and the anodic current measures the resultant rate of hydrogen release from reversible traps [32]. The difference between the experimental desorption curve and the theoretical one which fits the first part gives a measure of the reversible trapped hydrogen released from the anodic surface. Besides that, the experimental charge/discharge curves of a single specimen is not symmetrical and usually intercepts at $i/i_{max} = 0.10 \div 0.15$ instead of $i/i_{max} = 0.5$, as theoretically predicted by Fick's laws.

Charge transient:

Fourier transform:

$$\frac{i}{i_\infty} = 1 + 2\sum_{n=1}^{\infty}(-1)^n \exp\left(\frac{-n^2\pi^2 Dt}{L^2}\right) \quad (1)$$

Laplace transform:

$$\frac{i}{i_\infty} = \frac{2L}{\sqrt{\pi Dt}}\sum_{n=0}^{\infty}\exp\left[-\frac{(2n+1)^2L^2}{4Dt}\right] \quad (2)$$

Discharge transient:

$$(i/i_\infty)_{discharge} = 1 - (i/i_\infty)_{charge} \quad (3)$$

Evaluation of diffusion coefficients with partial charge and discharge method

In Fig. 8 the results of the partial charge (i_c from −0.5 to −1 mA/cm^2) and discharge (i_c from −1 to −0.5 mA/cm^2) tests of both X65 and F22 steel samples in different metallurgical microstructures are reported, together with the extreme theoretical curves.

Results are plotted with the usual parameters time/L^2 on *x*-axis and $\Delta i/\Delta i_{max}$ on *y*-axis, being Δi anodic current density minus quasi stationary anodic current density value reached during the previous charge.

Some relevant considerations can be discussed:

- every partial charge and discharge curve follows Fick's laws for their entire length, i.e., every transient can be completely described by only one parameter;
- for each sample and each partial charge/discharge couple the two experimental curves cross almost perfectly at the theoretical value $\Delta i/\Delta i_{max} = 0.5$, i.e., the diffusion coefficient of every couple of curves is about the same, which means that there is a high intrinsic reproducibility on the same specimen;
- diffusion coefficient values among different specimens of the same microstructure show a reduced dispersion and their values are reported in Table 6, in particular the scatter of *D* values is low in quenched and quenched and tempered specimens, it is higher in annealed material.

Table 6 – D_{max} and D_{min} values of partial charge/discharge method for different microstructures.

	Microstructures	D_{min} (10^{-11} m^2 s^{-1})	D_{max} (10^{-11} m^2 s^{-1})	D_{max}/D_{min}
X65	Annealed	120	330	2.75
	Quenched & Tempered	35	63	1.8
	Quenched	11	18	1.6
F22	Annealed	140	170	1.2
	Quenched & Tempered	62	66	1.07
	Quenched	16	24	1.50

From these considerations we should conclude that the value of D measured in this way is the lattice diffusion coefficient D_L even if we must remember that actually, according to Oriani [3], an almost ideal diffusion behaviour can be obtained in a material having only reversible traps with a very fast rate of the capture and release reactions, so in this case pure diffusion or diffusion plus trapping are not distinguishable.

Data from partial charge/discharge transients can be elaborated using the Fourier (Equation (1)) and Laplace (Equation (2)) methods.

According to Cheng [35], using the first term of the sum of Equation (1), the hydrogen diffusion coefficient can be derived from the slope of the plot of $\ln(1 - i/i_\infty)$ versus time (t):

$$\ln\left(1 - \frac{i}{i_\infty}\right) = \ln\left(2 - \frac{\pi^2 Dt}{L^2}\right) \tag{4}$$

In the same way, from the first term of Equation (2), D can be calculated from the slope of the plot of $\ln(It^{1/2})$ versus t^{-1} and from the Laplace constant:

$$\ln(It^{1/2}) = \text{constant} - \frac{L^2}{4Dt} \tag{5}$$

being the constant $\ln(2LI^\infty/\sqrt{\pi D})$, the D value can be also derived from the intercept of the plot of $\ln(It^{1/2})$ versus t^{-1}.

These methods allow to calculate D values from each single transient in different and independent ways, namely from: Fourier slope, Laplace slope, and Laplace constant of the linear section of the diagrams.

From each charge or discharge partial transient we always obtained experimental graphs presenting a rather long straight section therefore it was possible to calculate D values in four different ways, i.e. best fit of either Equation 1 or 2, and the three other methods indicated by Cheng [35].

The four D values calculated from the data of a single transient are very similar as it is exemplified for X65 steel sample in Fig. 9 where the best fit of partial charge/discharge D value is compared with the mean value calculated with the three other methods.

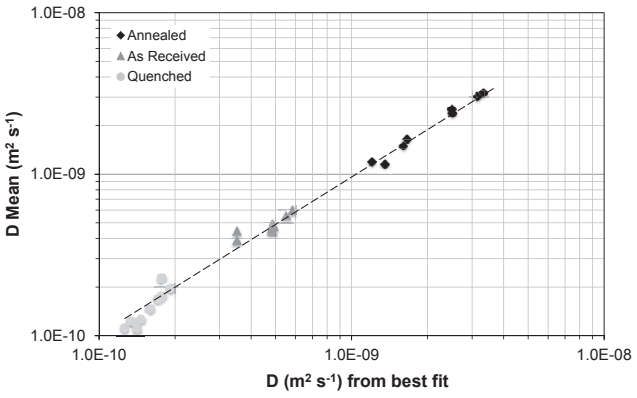

Fig. 9 – The average diffusion coefficient estimated from fourier slope, laplace slope and laplace constant (Y-axis) compared with the D value estimated from the best fit of the partial charge/discharge method (X-axis) for different steel microstructure of the X65 steel sample.

The attempt to apply Fourier and Laplace methods to the first complete permeation curves failed because:

1) in many cases it was not possible to detect a straight section in the curves obtained from experimental data;
2) when it was possible, the D values calculated with the different methods differed even by orders of magnitude.

Cathodic potentials during charge

In order to verify the cathodic behaviour of the material, potential was continuously measured. After the cathodic current switch off, potential started decreasing and only after tens of hours it stabilized. Although each single potential curve reached steady state value, data were scattered in ≈0.2 V band among different specimens even with the same microstructure.

In Fig. 10 the potential behaviour during partial charge and partial discharge is plotted, where the zero value of the time axis corresponds to the time of the cathodic current charge; one representative curve for each microstructure is presented.

Cathodic potential changes quickly after current density variation, then it maintains a constant value during the complete transient of the anodic current. Only quenched sample showed a little oscillation in a close range. Then, when the partial discharge started, a new stable value was reached almost immediately. This behaviour of the cathodic potential confirms that the procedure proposed by Zakroczymski [31,32], and here adopted, guarantees a constant hydrogen concentration on the cathodic side during the adsorption/desorption transients, which is fundamental for a correct diffusion coefficient measurement using the Devanathan and Stachurski method.

Effect of microstructure

In order to evaluate the effect of microstructure on the hydrogen permeation behaviour, the diffusion coefficient values obtained by the different methods were compared as follows:

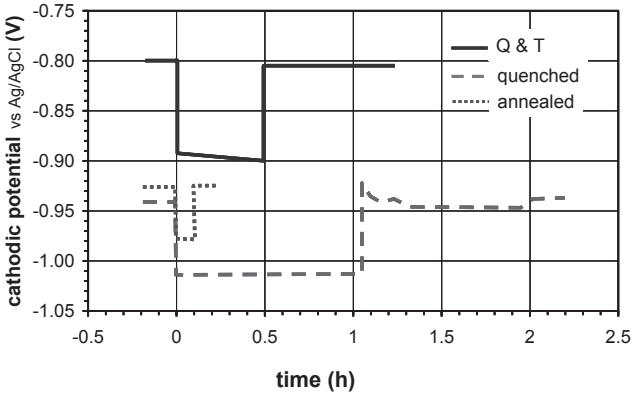

Fig. 10 – Cathodic potential registered during partial charge and partial discharge for one sample for each microstructure.

1. apparent diffusion coefficient, D_{app}, of complete charge method, according to ISO 17081 (both first and second charge);
2. diffusion coefficient, D_L, of partial charge/partial discharge method;
3. diffusion coefficient, D_L, calculated from the initial stage of desorption (i/i_{max} from 1 to 0.9).

Experimental data are summarized in Fig. 11 where the mean, maximum and minimum diffusion coefficient values measured with the different methods for each microstructure are reported. The following considerations arise:

- ISO 17081 charge method gives D values at least one order of magnitude lower than other methods;
- all other methods (partial charge/discharge and discharge) clearly show three bands of values in a reproducible way;
- the extreme D values found by desorption method are only slightly lower than the values obtained by partial method;
- the average value of D of partial charge/discharge and complete discharge methods for X65 grade steel are $13.2 \times 10^{-11}\ m^2\ s^{-1}$ in quenched, $38.2 \times 10^{-11}\ m^2\ s^{-1}$ in the as received one (about 2.8 times higher) and $181 \times 10^{-11}\ m^2\ s^{-1}$ in the annealed one (about 13.7 times higher);
- the average value of D of partial charge/discharge and complete discharge methods for F22 are $18.7 \times 10^{-11}\ m^2\ s^{-1}$ in quenched, $47.7 \times 10^{-11}\ m^2\ s^{-1}$ for the as received one (about 2.5 times higher) and $120 \times 10^{-11}\ m^2\ s^{-1}$ in the annealed one (about 6.5 time higher).

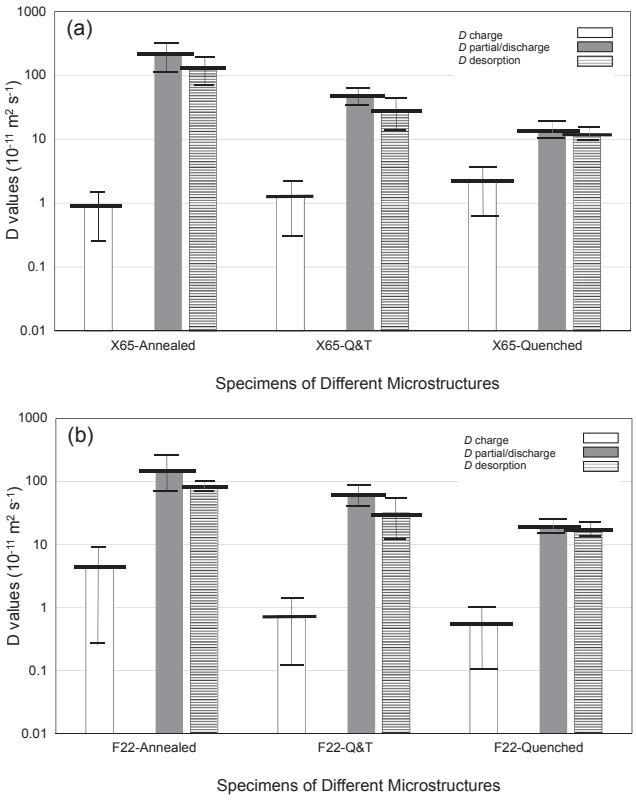

Fig. 11 – Diffusion coefficients measured on different microstructures of X65 (a) and F22 (b) with different methods; the average, min. and max. values are given.

From the point of view of the influence on the diffusion of hydrogen into steel, we can consider that the three microstructures studied show these general characteristics:

- the annealed microstructure has a ferritic (bcc) matrix, large grain size i.e. a limited extension of grain boundaries, a limited extension of different phase interfaces (interfaces between matrix and carbides in pearlite) and a low dislocation density;
- the quenched and tempered microstructure has a ferritic (bcc) matrix, small grain size i.e. a large extension of grain boundaries, a large extension of different phase interfaces (interfaces between matrix and precipitated carbides) and a relatively high dislocation density;
- the quenched microstructure has a body centered tetragonal (bct) matrix, small grain/platlet size i.e. a large extension of grain boundaries and a high dislocation density.

The measurement of diffusion coefficient according to ISO 17081 charge method is greatly affected by hydrogen trapping in many different sites, characterised by different trapping energies and kinetics (capture/release rates). Therefore in our experimental conditions with this method it was not possible to point out significant differences among diffusion coefficient of different microstructures.

Considering the diffusion coefficients measured by means of partial charge/discharge and discharge, our experimental tests clearly demonstrate a general trend of decreasing the diffusion coefficient with increasing the strength, in agreement with some literature results already mentioned in the introduction, see the results of paper [11,13,23] listed in Table 1. The trend found in our test is more reproducible and less scattered, probably due to the fact that in those papers apparent diffusion coefficient is normally measured.

Content and distribution of inclusions are almost the same for the different microstructures; hence, we can guess that grain boundaries and dislocations not only can act as hydrogen traps, but are also obstacles to its physical diffusion through the steel.

Sub-surface H concentration

An attempt to estimate diffusible and reversibly trapped hydrogen has been made in one of tested steel (API 5L X65) in the three different metallurgical microstructures.

The quantity of hydrogen that is contained in the specimens, near the cathodic surface during the tests, in particular the sub-surface concentration of lattice hydrogen (C_{H0}) can be calculated from Fick's first law:

$$C_{H0} = (I_{SS} \cdot L)/D$$

where I_{SS} is the steady state current immediately before the discharge, D is the diffusion coefficient calculated for the initial stage of the discharge curve. The mean value of the estimated sub-surface concentration of lattice hydrogen are: 0.1 ppm in the annealed material, 0.3 ppm in the Q&T one and 0.6 ppm in the quenched one, i.e. for our material, at stationary electrochemical conditions, the lower is the diffusion coefficient the higher is the concentration of

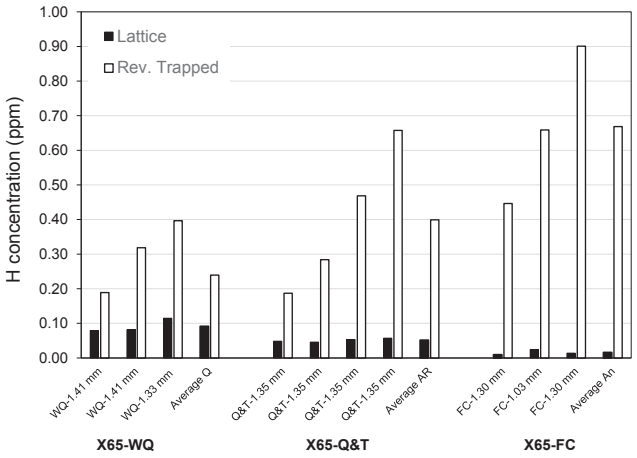

Fig. 12 – Lattice and reversibly trapped hydrogen concentration of different specimens estimated from hydrogen discharge transients of the anodic surface for X65 steel microstructures.

absorbed atomic hydrogen in equilibrium with the one developed by cathodic reaction. This same tendency can be found in Luu and Wu [34] on carbon steel and in Haq [11] on an X70 pipeline steel.

Lastly, integration of the experimental and theoretical (best fit of the initial stage) desorption transients of different steel microstructures has been performed in order to quantify the amount of hydrogen in lattice and reversible. Fig. 12 exemplified the results of this evaluation for the X65 specimens; for studied steels the concentration of hydrogen in lattice sites is in the order of: quenched > quenched and tempered > annealed.

On the other hand, the reversibly trapped hydrogen was higher in the annealed sample compared with other ones and it constitutes a majority of the total amount of absorbed hydrogen; the average value being 97.6% for annealed sample, 87.2% for Q&T, and 69.5% for quenched one. The last obtained results in the case of annealed sample are in agreement with Zakroczymski et al. [31,32].

The data of Fig. 12 are scattered then they must be considered only as qualitative indication and not in absolute terms but rather relative to each other. Also taking into consideration that the measured discharge curve refers to the hydrogen flowing out from the anodic surface; due to the experimental solutions adopted in our tests it was not possible to measure also the amount of hydrogen escaping from the cathodic surface that is about 2 times the anodic contribution according Nanis and Namboodhiri [30].

Conclusions

In the experimental work here presented, the application of the procedure of partial charge/discharge, allows to obtain permeation curves that follow the theoretical behaviour predicted by Fick's laws and can be completely described by a single constant diffusion coefficient *D*, close to the one of pure iron that can be reasonably assumed to be the lattice diffusion coefficient. These conclusions are confirmed by the results of complete discharge curves that, in their first section, can be interpolated by a theoretical Fick's solution giving a *D* value very close to the one obtained by the method of partial charge/discharge. Lattice diffusion coefficient is higher and more reproducible than the apparent *D* obtained using the ISO approach (1st and 2nd charge). The partial charge/discharge method gave a clear distinction between different steel microstructures and the results, which are evaluated with four different and independent ways: best fit of the experimental transient, Fourier slope, Laplace slope, and Laplace constant of the linear section of the diagrams were in agreement.

The partial charge/discharge method has been applied to measure diffusion coefficient of a C–Mn X65 and low alloy F22 steel in three different microstructures: annealed, "as received" (i.e., quenched & tempered) and quenched. The hydrogen diffusion coefficient decreases as steel hardness increases, in particular the average values for X65 are: $22.5 \cdot 10^{-10}$ m^2 s^{-1} for the annealed microstructure, $4.9 \cdot 10^{-10}$ m^2 s^{-1} for the quenched and tempered one and $1.4 \cdot 10^{-10}$ m^2 s^{-1} for the martensitic one. In the same way, for F22: $15.5 \cdot 10^{-10}$ m^2 s^{-1} for the annealed, $6.4 \cdot 10^{-10}$ m^2 s^{-1} for quenched and tempered, and $2.0 \cdot 10^{-10}$ m^2 s^{-1} for the martensitic one.

REFERENCES

[1] Devanathan MAV, Stachurski Z. The adsorption and diffusion of electrolytic hydrogen in palladium. Proc Roy Soc A 1962;270:90.

[2] McNabb A, Foster PK. A new analysis of the diffusion of hydrogen in iron. J Trans Metall Soc AIME 1963;227:618–27.

[3] Oriani RA. The diffusion and trapping of hydrogen in steel. Acta Metall 1970;18:147–57.

[4] Iino M. A more generalized analysis of hydrogen trapping. Acta Metall 1982;30:367–75.

[5] Iino M. Analysis of irreversible hydrogen trapping. Acta Metall 1982;30:377–83.

[6] Péter L, Almási B, Verő B, Schneider H. Theoretical analysis of entrapment kinetics in hydrogen permeation experiments. Mat Sci Eng A 2003;339:245–54.

[7] Leblond JB, Dubois D. Overview no. 29 A general mathematical description of hydrogen diffusion in steels – I. Derivation of diffusion equations from Boltzmann-type transport equations. Acta Metall 1983;31(10):1459–69.

[8] Leblond JB, Dubois D. "Overview no. 29 A general mathematical description of hydrogen diffusion in steels – II. Numerical study of permeation and determination of trapping parameters. Acta Metall 1983;31(10):1471–8.

[9] Turnbull A, Carroll MW, Ferriss DH. Analysis of hydrogen diffusion and trapping in a 13% chromium martensitic stainless steel. Acta metall 1989;37:2039–46.

[10] ISO 17081. Method of measurement of hydrogen permeation and determination of hydrogen uptake and transport in metals by an electrochemical technique. 1st ed. 2004.

[11] Haq J, Muzaka K, Dunne DP, Calka A, Pereloma EV. Effect of microstructure and composition on hydrogen permeation in X70 pipeline steels. Int J Hydrogen Energy 2013;38:2544–56.

[12] Turnbull A, Saenz De Santa Maria M, Thomas ND. The effect of H_2S concentration and pH on hydrogen permeation in AISI 410 stainless steel IN 5% NaC1. Corros Sci 1989;29:89–104.

[13] Park GT, Koh SU, Jung HG, Kim KY. Effect of microstructure on the hydrogen trapping efficiency and hydrogen induced cracking of linepipe steel. Corros Sci 2008;50:1865–71.
[14] Dong CF, Li XG, Liu ZY, Zhang YR. Hydrogen-induced cracking and healing behaviour of X70 steel. J Alloys Compd 2009;484:966–72.
[15] Dong CF, Liu ZY, Li XG, Cheng YF. Effects of hydrogen-charging on the susceptibility of X100 pipeline steel to hydrogen-induced cracking. Int J Hydrogen Energy 2009;34:9879–84.
[16] Kappes M, Frankel GS, Yhodla R, Mueller M, Sridhar N, Carranza RM. Hydrogen permeation and corrosion fatigue crack growth rates of X65 pipeline steel exposed to acid brines containing thiosulfate or hydrogen sulfide. Corrosion 2012;68:1015–28.
[17] Bolzoni F, Cabrini M, Spinelli C. Hydrogen diffusion and hydrogen embrittlement behaviour of two high strength pipeline steels. In: Proc of Eurocorr 2001, Riva del Garda, Italy; 2001.
[18] Cabrini M, Cogliati O, Maffi S. Effect of microctructure on hydrogen diffusion in carbon steels (Effetto della microstruttura sulla diffusione dell'idrogeno in acciai al carbonio per pipeline). La Metall Ital 2003;95(3):13–20.
[19] Cabrini M, Lorenzi S, Marcassoli P, Pastore T. Effetto della diffusione dell'idrogeno sui fenomeni di EAC di acciai per pipeline in condizioni di protezione catodica. La Metall Ital 2008;100(2):15–22.
[20] Serna S, Martinez H, Lopez SY, Gonzalez-Rodriguez JG, Albarran JL. Electrochemical technique applied to evaluate the hydrogen permeability in microalloyed steels. Int J Hydrogen Energy 2005;30:1333–8.
[21] Asher S, Singh PM, "Hydrogen production and permeation in near-neutral pH environments", Corros NACE 2008, Paper Nr. 08411.
[22] API Specification 5L. Specification for line pipe; 2004.
[23] Parvathavarthini N, Saroja S, Dayal RK, Khatak HS. Studies on hydrogen permeability of 2.24% Cr-1% Mo ferritic steel: correlation with microstructure. J Nucl Mater 2001;288:187–96.
[24] Yazdipour N, Haq AJ, Muzaka K, Pereloma EV. 2D modelling of the effect of grain size on hydrogen diffusion in X70 steel. Comput Mater Sci 2012;56:49–57.
[25] Fallahmohammadi E, Bolzoni F, Lazzari L. Measurement of lattice and apparent diffusion coefficient of hydrogen in X65 and F22 pipeline steels. Int J Hydrogen Energy 2013;38:2531–43.
[26] Fassina P, Morana R, Alleva L, Mortali G, Vergani L. Materials behavior in extreme conditions: influence of large amounts of H_2S on steel toughness in arctic environments. In: Proc EUROCORR 2010, Moscow, Russia; 2010.
[27] Bolzoni F, Fassina P, Fumagalli G, Lazzari L, Re G. Hydrogen charging of carbon and low alloy steel by electrochemical methods. In: Proc EUROCORR 2010, Moscow, Russia; 2010.
[28] Fassina P, Bolzoni F, Fumagalli G, Lazzari L, Vergani L, Sciuccati A. Influence of hydrogen and low temperature on pipeline steels mechanical behaviour of two pipeline steels. Eng Fract Mech 2012;81:43–55.
[29] Fassina P, Brunella F, Lazzari L, Re G, Vergani L, Sciuccati A. Effect of hydrogen and low temperature on fatigue crack growth of pipeline steels. Eng Fract Mech 2013;103:10–25.
[30] Nanis L, Namboodhiri TKG. Mathematics of the electrochemical extraction of hydrogen from iron. J Electrochem. Soc V 1972;119:691–4.
[31] Zakroczymski T. Adaptation of the electrochemical permeation technique for study entry, transport and trapping of hydrogen in metals. Electrochim Acta 2006;Vol. 51:2261–6.
[32] Zakroczymski T. Electrochemical determination of hydrogen in metals. J Electroanal Chem 1999;475:82–8.
[33] Frappart S, Feaugas X, Creus J, Thebault F, Delattre L, Marchebois H. Study of the hydrogen diffusion and segregation into Fe–C–Mo martensitic HSLA steel using electrochemical permeation test. J Phys Chem Solids 2010;71:1467–79.
[34] Luu WC, Wu JK. The influence of microstructure on hydrogen transport in carbon steels. Corros Sci 1996;38:239–45.
[35] Cheng YF. Analysis of electrochemical hydrogen permeation through X-65 pipeline steel and its implications on pipeline stress corrosion cracking. Int J Hydrogen Energy 2007;32:1269–76.
[36] Kim WK, Koh SU, Yang BY, Kim KY. Effect of environmental and metallurgical factors on hydrogen induced cracking of HSLA steels. Corros Sci 2008;50:3336–3342,.
[37] Scoppio L, Barteri M. Methods of hydrogen uptake measurements by electrochemical permeation test on low alloy steels. In: Turnbull A, editor. Hydrogen transport and cracking in metals. Proceedings of a conference, Teddington UK; 1995. 204–215,.
[38] Andenna C, Torella RA. Study of hydrogen permeation on API X65 TMCP steel under stress conditions. In: Turnbull A, editor. Hydrogen transport and cracking in metals. Proceedings of a conference, Teddington UK; 1995. pp. 240–52.
[39] Xue HB, Cheng YF. Characterization of inclusions of X80 pipeline steel and its correlation with hydrogen-induced cracking. Corros Sci 2011;Vol. 53:1201–1208,.
[40] Olden V, Alvaro A, Akselsen OM. Hydrogen diffusion and hydrogen influenced critical stress intensity in an API X70 pipeline steel welded joint. Experiments and FE simulations. Int J Hydrogen Energy 2012;37:11474–86.
[41] Ramunni VP, De Paiva Coelho T, de Miranda PEV. Interaction of hydrogen with the microstructure of low-carbon steel. Mat Sci Eng 2006;435–436:504–14.